ACS APPLIED NANO MATERIALS

www.acsanm.org Article

Mesomorphic Ceramic Films Synthesized *via* Lyotropic Self-Assembly of Metal Oxide Nanorods Complete with Sintering

Wenshi Zhang, Shaw H. Chen, James N. Hilfiker, and Mitchell Anthamatten*

Cite This: https://dx.doi.org/10.1021/acsanm.0c01668 Read Online

ACCESS | Metrics & More | Article Recommendations | Supporting Information

ABSTRACT: Mesomorphic ceramics are broadly defined as solid systems with morphologies intermediate between isotropic materials and single crystals. To illustrate this materials concept, a class of mesomorphic ceramics with nematic-like superstructures has been synthesized *via* lyotropic liquid crystals of titanium dioxide, TiO_2, in an isotropic solvent for a demonstration of uniaxially oriented solid films. A lyotropic dispersion of ligand-capped anatase nanorods at 60 wt % in chlorobenzene was calcined and sintered with prior manual shear to form an optically anisotropic, 2.3 ± 0.3 μm-thick solid film. In the course of sintering, nanorods fuse into low-aspect ratio grains that form nematic domains. Shear-induced alignment of nanorods followed by thermal treatment creates uniaxial orientation across millimeters, which exhibits high optical transparency and a nearly constant birefringence of 0.018 ± 0.002 from 650 to 1700 nm. Distinct from liquid-crystal templating, this new approach yields superstructures of nanoparticles with relative ease and at lower costs. The present study opens a pathway toward robust, ceramic-based solid films for diverse application.

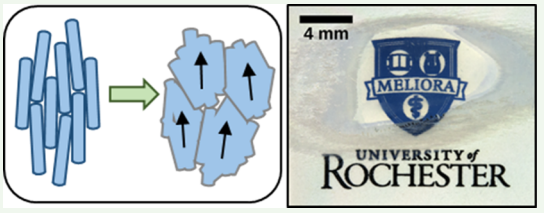

KEYWORDS: *nanorods, lyotropic liquid crystals, sintering, oriented transparent ceramics, waveplates*

INTRODUCTION

Since their invention in the 1960s, lasers have served diverse technologies, many of which benefit from polarization control, beam shaping, and polarization smoothing that underlie laser-based devices for optical communications,[1−3] laser power scaling,[4] and biological and medical imaging,[5,6] to name a few. With the ease of device scale-up at affordable costs, liquid crystal devices have become essential for polarization control, including circular and linear polarizers, and waveplates, using, in particular, cholesteric and nematic classes that are readily processed into large-area defect-free films. To improve device robustness with morphological stability against crystallization spanning decades, glassy liquid crystals emerged as a superior material class in the early 1990s *via* vitrification of liquid crystals below their glass transition temperatures without altering morphology.[7,8] Various device concepts have been successfully tested using selected materials, including nonabsorbing polarizers, notch filters and reflectors, polarized electroluminescence, and solid-state lasers, all showing commendable performance levels. Simultaneously, sculptured thin-film devices have been actively explored by glancing angle deposition (GLAD) of metal oxide physical vapors to further improve optical device robustness by virtue of the inorganic constructs.[9,10] Additional transparent, ceramic-based materials have also emerged, attracting a great deal of attention for their potential to offer high laser damage resistance.[11,12]

Mesomorphism represents the state of matter intermediate between isotropy and three-dimensional (3D) crystallinity. Examples of mesomorphism include molecular-scale liquid crystallinity characterized by order in one or two dimensions (2D), nanometer-scale helical coils generated by GLAD, and textured ceramics defined as the polycrystalline material with the preferred crystallographic orientation of grains.[13,14] This study is inspired by the realization that liquid crystals can form nematic and cholesteric mesophases through self-organization of rodlike molecular entities in uniaxially oriented and helically stacked structures, respectively.[15,16] In particular, the present study aims at a class of mesomorphic ceramics with nematic-like superstructures and optical properties originating from lyotropic self-assembly of titanium dioxide (TiO_2) nanorods. The underlying idea is to transition from molecular-scale nematogens to nanometer-scale TiO_2 nanorods as mesomorphic building blocks. The resulting liquid-crystal-like superstructures and optical properties are expected to be preserved in the solid state *via* sintering, that is, interparticle atomic diffusion driven by the reduction in surface Gibbs energy. Our unique approach leverages established methods for functionalizing anatase TiO_2 nanorods[17] and aligning nanorods[18−20] to serve as a new strategy for the fabrication of inorganic, anisotropic films. Anatase TiO_2 nanorods are chosen for illustration because of their facile synthesis, and their crystalline *c*-axis is oriented along

Received: June 17, 2020
Accepted: October 8, 2020

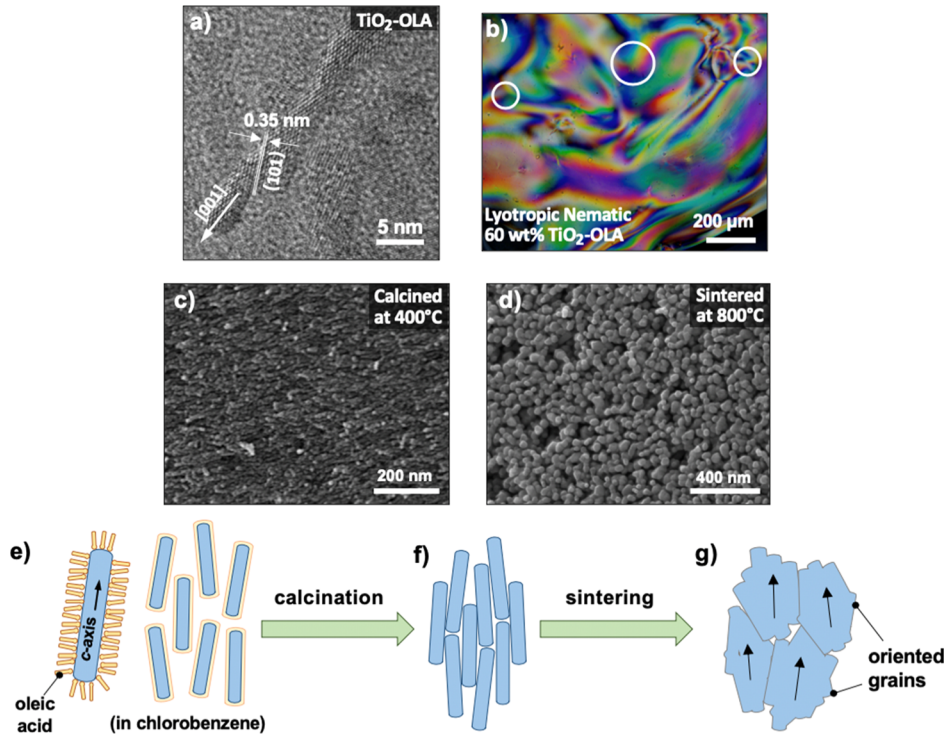

Figure 1. Schematic showing the fabrication of mesomorphic ceramics with electron and optical microscopic images without substrate surface treatment: (a) transmission electron microscopic image of oleic acid-capped TiO_2 nanorods, (b) polarized optical microscopy images of the lyotropic nematic mesophase at 60 wt % oleic acid-capped nanorods in chlorobenzene with white circles identifying Schlieren brush textures, (c) assembled nanorods after calcination at 400 °C for 2 h (SEM) and (d) after sintering at 800 °C for 2 h (SEM), and (e−g) schematic depicting lyotropic nematic assembly of oleic acid-capped TiO_2 nanorods followed by calcination and sintering to create a nearly monodomain nematic-like film.

the nanorod axis, affording intrinsic birefringence upon alignment. Moreover, nematic lyotropic mesomorphism of oleic acid-functionalized TiO_2 nanorods dispersed in chlorobenzene has been demonstrated.[19] Also, distinct from the use of liquid crystal fluids as templates to create a solid superstructure of nanoparticles,[21] our approach employs an isotropic, volatile solvent to facilitate material processing. Beyond polarization control, the manipulation of the microstructure of inorganic ceramics is crucial for advancing a diversity of applications including photocatalysis,[22,23] dye-sensitized solar cells,[24,25] field-effect transistors,[26] and piezoelectric ceramics.[27,28]

EXPERIMENTAL SECTION

Synthesis of Oleic Acid-Capped TiO_2 Nanorods. A reaction mixture was prepared with oleic acid (Alfa Aesar, 90%), titanium tetraisopropoxide (TTIP, Sigma-Aldrich, 99.999%), and trimethylamino-*N*-oxide (TMAO, Alfa Aesar, 98+%). The oleic acid-capped TiO_2 nanorods (TiO_2-OLA) were synthesized following a published procedure.[17,19] Oleic acid (140 g) was heated at 120 °C under vacuum for 1 h to remove residual water and cooled to 90 °C followed by injection of TTIP (5.7 g, 20 mmol). After stirring for 10 min, 2 M aqueous solution (20 mL) of trimethylamino-*N*-oxide was quickly injected. The reaction mixture was then heated at 100 °C for 48 h under Ar flow. After cooling to room temperature, the reaction mixture was dried under vacuum to remove water. About 400 mL of methanol was then added, the resultant precipitate was separated through three centrifugation cycles (14,500 rpm, 15 min). The final product was dried and dispersed in chlorobenzene to form a 10 wt % transparent colloidal dispersion.

Formation of the Lyotropic Nematic Mesophase. Following the procedure reported by Cheng *et al.*,[19] a dispersion of 10 wt % TiO_2-OLA in chlorobenzene was allowed to slowly evaporate at room temperature while being observed under a polarized optical microscope. Evaporation continued until a desired concentration of 55−65 wt % was reached, as determined gravimetrically. Gel formation was avoided by applying sonication and adding up to 10 wt % extra oleic acid. Once a highly birefringent mesophase was observed, the sample was sandwiched between a microscope glass slide and a cover slip for observation and processing. For the samples treated at 600 °C or higher, quartz substrates were employed instead of glass substrates and cover slips.

Fabrication and Orientation of Mesomorphic Ceramics. A sandwiched cell containing a lyotropic assembly of nanorods was transferred into a box furnace (Lindberg, Blue M) for thermal treatment. The furnace was programmed to ramp at 1 °C min^{-1} to a specified temperature for continuous heating over 2 h. Uniaxially aligned samples were fabricated by manually applying shear forces to lyotropic dispersions (at 60 wt % TiO_2-OLA in chlorobenzene) between one surface-treated quartz substrate and one bare quartz substrate. Following the application of shear, thermal treatment was performed as described above.

Quartz Substrate Surface Treatment. An adhesion promoter P20, consisting of 20% hexamethyldisilazane (Polysciences Inc.) and 80% propylene glycol monomethyl ether acetate (Transene Company, Inc.), and a positive photoresist (MICROPOSIT S1805) were successively spin-coated (500 rpm, 5 s; 3000 rpm, 60 s; 500 rpm, 5 s) onto a precleaned quartz substrate. After soft baking at 115 °C for 60 s, direct-write laser photolithography (Microtech, LW405) was performed to generate the desired pattern (1 cm × 1 cm) with the parallel lines (1 cm long, 5 μm wide) of 5 μm spacings under an exposing power of 135 mJ cm^{-2}. The substrates were then developed with the developer (MICROPOSIT MF-319) for 20−40 s and rinsed with water followed by blow drying with N_2. Hard baking was then performed at 115 °C for 120 s before reactive ion etching (South Bay Technology, reactive ion etcher RIE-2000) under a gas mixture (O_2: 15 SCCM, CHF_3: 10 SCCM, and SF_6: 30 SCCM) for 2−4 min. The residual photoresist was rinsed off with acetone to obtain a trenched

https://dx.doi.org/10.1021/acsanm.0c01668
ACS Appl. Nano Mater. XXXX, XXX, XXX−XXX

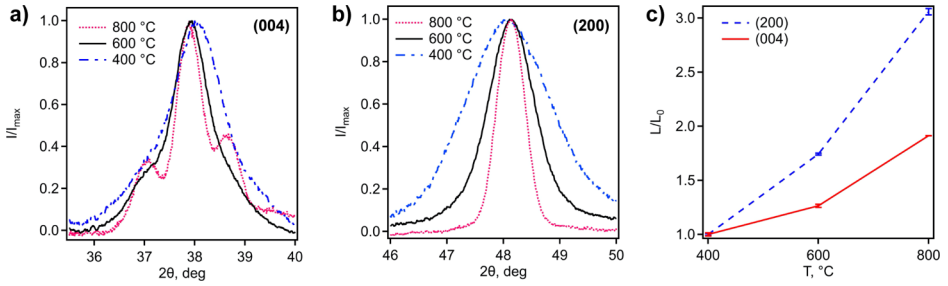

Figure 2. Narrowing of X-ray diffraction peaks as a result of sintering assemblies of titania nanorods without substrate surface treatment: (a,b), normalized intensities *vs* 2θ for the crystallographic (004) and (200) planes and (c) relative crystallite size after thermal treatment. The relative crystallite size was derived from the Debye−Scherrer equation for different crystal planes, as described in the text. Errors in the plot correspond to the 95% confidence intervals of parameters used to fit diffraction peaks.

pattern substrate with a depth of 110−150 nm and a width of 5 μm verified using a profilometer (Ambios XP-200 surface profiler).

Characterization. The morphology, crystalline structure, and optical properties of the oleic acid-capped TiO_2 nanorods and calcined and sintered products were extensively characterized. For thermogravimetric analysis (TGA, TA Instruments, Q5000), samples were dried under vacuum at 50 °C overnight and *in situ* at 120 °C under N_2 for 1 h right before collecting the TGA scans at 20 °C min^{-1} from 120 to 650 °C under air. Bright-field transmission electron microscopy (TEM, FEI Tecnai F20 G2) was employed to characterize oleic acid-capped TiO_2 nanorods at a voltage of 200 kV, and scanning electron microscopy (Zeiss, Auriga) at 5 kV under the InLens mode was employed for characterizing surface morphology after calcination and sintering. Polarizing optical microscopy (Leica, DM LM/P) was performed to observe the birefringent texture of samples. X-ray diffraction was performed using an XtaLAB Synergy-S diffractometer (Rigaku) with a 2D HyPix-6000HE HPC detector, and data were analyzed using CrysAlis^{Pro} (Rigaku) and Data Squeeze (University of Pennsylvania). To determine the crystalline structure, X-ray diffraction (XRD) was performed using Cu Kα X-rays with a sample-to-detector distance of 31.2 mm and an exposure time of 10 min. To analyze the preferred orientation of crystallites, single flakes with lateral dimensions of 100−200 μm were mounted with the shearing direction oriented normal to the incident beam, and XRD was performed to a higher q-range using Mo Kα X-rays at a distance of 36.5 mm and an exposure time of 5 min. Brunauer−Emmett−Teller (BET) (Micromeritics, ASAP 2020) analysis was conducted to measure the specific surface area of the calcined and sintered samples. The bulk sample for BET analysis was dried in a vacuum oven overnight before ramping at 20 °C min^{-1} to the target temperature and held there for 2 h. A UV−vis−NIR spectrometer (PerkinElmer, Lambda 900) was employed to measure the transmission spectrum of the sintered sample between a pair of quartz substrates relative to a reference cell consisting of the same substrates with an air gap. Spectroscopic Mueller-matrix ellipsometry (J. A. Woollam, RC2) measurements were collected at variable angles in transmission to obtain the film thickness and optical birefringence of the sintered sample.

RESULTS AND DISCUSSION

Nanorod Synthesis and Lyotropic Assembly. As building blocks for the mesomorphic ceramics, oleic acid-capped TiO_2 nanorods were synthesized in one pot through hydrolysis of titanium tetraisopropoxide in oleic acid under mild conditions.[17] Nanorods were characterized as the anatase phase by XRD (Figure S1), and the shape and dimension of the single crystallite nanorods were characterized by TEM, as shown in Figures 1a and S2.[17] The nanorods' length and aspect ratio are estimated at 20 to 30 nm and 5 to 8, respectively, similar to those previously reported.[19] Moreover, consistent with a previous report,[17] the c-axis of the TiO_2 anatase phase is oriented along the nanorod long axis, as shown by the high-resolution TEM image in Figure 1a, where the (101) plane is labeled to identify the anatase phase.[17,29] According to the TGA thermograms compiled in Figure S3, the ligand-capped nanorods contain 24 wt % oleic acid. A large amount of oleic acid was applied to ensure a stable dispersion following the previous work by Cheng *et al.*[19]

The as-synthesized oleic-acid-capped anatase nanorods were readily dispersed in chlorobenzene to yield temporally stable lyotropic nematic liquid crystals, as described in the Experimental Section. The image in Figure 1b shows a birefringent texture observed at room temperature between glass substrates of nanorods dispersed at 60 wt % in chlorobenzene. Such a concentration was necessary to ensure nematic mesomorphism.[19] The Schlieren texture is consistent with a lyotropic nematic mesophase, which is further supported by its response to shear and the rotation of brush disclinations both with and counter to stage rotation; see Figure S4.[30] The sandwiched samples containing lyotropic dispersions were subjected to thermal treatments. Following thermal treatment at 400 °C for 2 h to completely remove the oleic acid ligands,[31] the material appears as a brittle solid, and flakes inspected under SEM reveal a dense, anisotropic morphology, shown in Figure 1c, comprising preferentially oriented features with dimensions comparable to those of the pristine nanorods. To solidify the anisotropic microstructure from the lyotropic phase into a continuous film, thermal treatments at both 600 and 800 °C were performed for 2 h each. Based on TGA data, the resulting mesomorphic ceramics contain neither the residual solvent nor oleic acid. Figure 1d shows the SEM image of grains ranging from 25 to 75 nm, as determined in Figure S5, following thermal treatment at 800 °C. The SEM image of the same film at higher magnification is displayed in Figure S6a and shows angular facets as the evidence of crystallinity with further validation of crystallinity by XRD in Figure 2. A similar morphology is observed for the cross section in Figure S6b. Schematically, the process begins with lyotropic ordering of single crystallite nanorods, captured in Figure 1e,f, and the neighboring nanorods are fused to form crystalline grains, as depicted in Figure 1g, characterized as sintering. There are hitherto unknown factors during thermal processing and the removal of oleic acid that may lead to pores and defects speculated herein. The final product consists of mesomorphic ceramic domains with preferentially aligned crystallographic axes to be elaborated as follows.

Thermal Sintering. The sintering process was analyzed by both XRD and specific surface area measurement. The samples treated at 400, 600, and 800 °C were characterized as anatase, as by XRD data shown in Figure S7. Bragg diffraction peaks for the (004) and (200) planes narrow upon thermal treatment, as

https://dx.doi.org/10.1021/acsanm.0c01668
ACS Appl. Nano Mater. XXXX, XXX, XXX−XXX

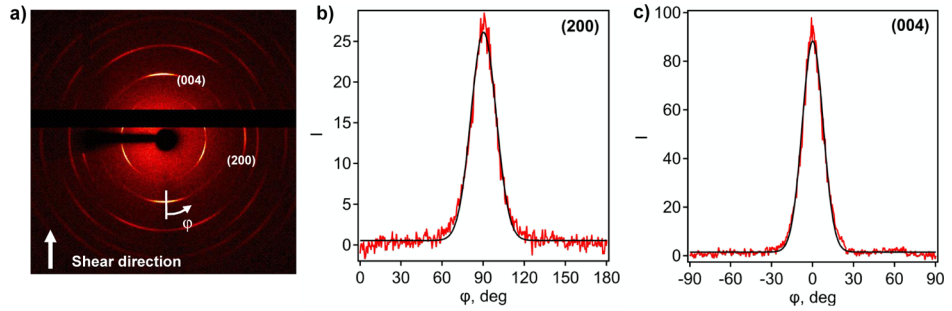

Figure 3. Wide-angle X-ray diffraction data acquired from a sintered mesomorphic ceramic flake sheared on a surface-treated substrate showing the preferred orientation of crystal planes: (a) 2D diffraction pattern; (b) azimuthal scan for the (200) crystal plane of anatase, 3.28 $nm^{-1} < q < 3.36$ nm^{-1} ($q = 4\pi \sin\theta/\lambda$); and (c) azimuthal scan for the (004) crystal of anatase, 2.61 $nm^{-1} < q < 2.69$ nm^{-1}. Red traces in (b,c) indicate measured intensity, and black curves are fitted Gaussians to determine the degree of the orientational order.

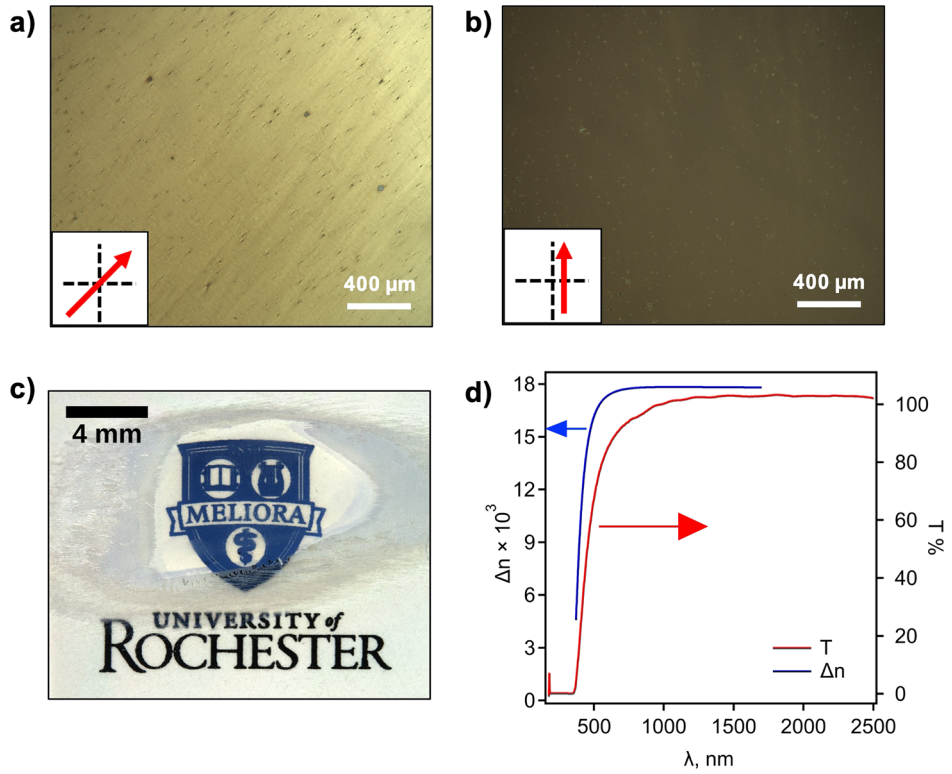

Figure 4. Optical properties of the shear-aligned and sintered ceramic film between one surface-treated quartz substrate and the other untreated substrate: POM images taken with respect to the shearing direction (a) oriented 45° and (b) parallel to cross polarizers, identical to those shown in Figure S8 for a lyotropic nematic film before thermal treatments; (c) photograph of a shield logo placed behind the sandwiched specimen demonstrating optical transparency; and (d) UV−vis−NIR transmission spectrum and optical birefringence dispersion of 2.3 μm-thick films.

shown in Figure 2, suggesting that the anatase crystallites grow upon treatment at increasing temperatures (*e.g.*, 400, 600, and 800 °C), consistent with the grain coarsening shown in Figure 1d. It is noted that anatase crystallinity persists from the freshly prepared nanorods at 800 °C. Sintering was also evident from the specific surface area quantified by the BET technique, which indicates significantly reduced values from 305 to 74 m^2 g^{-1} following the treatment at 400 and 600 °C, respectively. Thus, the XRD and BET analyses combine to indicate sintering as a continual process from 400 °C and so on. The optical transparency of the sample sintered at 600 °C was observed to be inferior to that following sintering at 800 °C, which also resulted in improved resistance to cracking.

In addition, XRD analysis was employed to probe the reduction in shape anisotropy upon sintering at high temperatures as a corroboration for the SEM images in Figure 1c,d. The change in length scale of a crystallite dimension normal to a selected diffraction plane can be calculated from the Debye−Scherrer equation as $L = K\lambda/\beta \cos\theta$, where K is a shape constant, λ is the wavelength of the X-ray beam, θ is the Bragg angle, and β is the full width at half-maximum, fwhm, of the selected diffraction peak. Figure 2c shows the relative changes in sizes, L/L_0, where L_0 is the crystallite dimension after thermal treatment at 400 °C, for both the (200) and (004) planes. As a result of sintering, the average dimension normal to the crystallite's (200) plane nearly triples, and the average dimension normal to the (004) plane nearly doubles. Because the *c*-axis lies along the long axis of the nanorods, these observations indicate that nanorods tend to fuse together primarily in the lateral direction during sintering. This explains the loss in shape anisotropy of crystalline

https://dx.doi.org/10.1021/acsanm.0c01668
ACS Appl. Nano Mater. XXXX, XXX, XXX−XXX

grains after sintering at 800 °C, as also observed in the SEM image in Figure 1d.

Macroscopic Shear Alignment and Optical Properties. Liquid crystalline dispersions were processed from a polydomain lyotropic phase, such as that shown in Figure 1b, into an oriented lyotropic nematic monodomain by manual shear on a surface-treated substrate followed by sintering. To evaluate the potential to serve as optical waveplates, the preferred orientation of a shear-aligned, mesomorphic ceramic film sintered at 800 °C was characterized using wide-angle X-ray diffraction. Figure 3a shows the 2D-XRD pattern of a flake that was oriented orthogonal to the beam, with the shear direction vertically aligned. The 2D-XRD pattern is consistent with the uniaxial orientation along the *c*-axes of the grains formed from fused nanorods and shows an orientational order of crystallographic planes parallel (200) and perpendicular (004) to the grain's *c*-axis. Figure 3b,c displays the azimuthal variation in intensity for the (200) and (004) planes. Part of the detector was unavoidably blocked by the beamstop. To circumvent this effect in the analysis of the full azimuthal intensity profile, the sample was rotated azimuthally in 45° increments, and the collected data were averaged. The preferred orientation is characterized by the degree of orientational order defined as $f = [180° - \text{fwhm}]/180°$, where fwhm in degrees is calculated from a least-squares fit to the Gaussian function.[32] The calculated f values at 0.88 and 0.90 for the (200) and (004) planes, respectively, signify good alignment of the anatase crystallites' *c*-axes along the shear direction.

The optical properties of a macroscopically aligned mesomorphic ceramic film were further investigated, as shown in Figure 4. When viewed under crossed polarizers, optical birefringence of the shear-aligned and sintered film extends over millimeter dimensions, whereas birefringent domains without prior shear are less than 200 μm. Figure 4a,b shows light transmission through crossed polarizers if the sample shear direction is oriented to be 45° to a polarizer, while extinction is observed if the shear direction is aligned along either polarizers. These observations indicate that the film displays in-plane birefringence over millimeters, which originates from the lyotropic nematic assembly. It appears that the preferred orientation of nanorods imparted by shearing was preserved upon sintering, forming a nematic-like superstructure with permanent, in-plane birefringence. The mesomorphic ceramic film sandwiched between two quartz substrates exhibits excellent transparency over the millimeter length scale, as shown in Figure 4c. Haziness is present in the surrounding regions which are attributed to cracks from the gaps or voids, whereas the transparent region is in good contact with the substrates. The UV−vis−NIR transmission spectrum, in Figure 4d, shows optical transparency from 1000 to 2500 nm. Note that transmission appears to exceed 100% presumably because Fresnel reflection from the mismatch of refractive indices between the ceramic film and the quartz substrates is not fully accounted for by the empty reference cell. Assuming that the average refractive index of the mesomorphic ceramics film is about 1.7 and that of the substrate is 1.5, the overall Fresnel loss is estimated at 8.8%, while the Fresnel loss from the two substrates with an air gap in the middle is 16%. Thus, the presented transmission is about 7.2% higher than it should be. The high transparency is attributed to the small crystalline grains size and small pore size that limits losses because of scattering, as shown in Figures 1d and S9.[33]

The film thickness and optical birefringence of the same mesomorphic ceramic film were independently determined by measuring the Mueller matrix in the transmission mode, MMt, at varying incidence angles followed by analysis with the biaxially anisotropic model.[34] The dielectric function along each orientation was described using a Kramers−Kronig consistent Sellmeier dispersion relation,[35] with one orientation including Gaussian absorption to describe the onset of absorption before the film became opaque at shorter wavelengths. The thickness was determined to be 2.3 ± 0.3 μm by matching the coherent oscillations at an oblique incident angle.[36] Much of this uncertainty is due to the nonuniformity of the film across the measured beam, which was considered in the model. The wavelength dispersion of optical birefringence is shown in Figure 4d, which indicates a nearly constant optical birefringence, $\Delta n = n_{\parallel} - n_{\perp} = 0.018 \pm 0.002$ at wavelengths exceeding 650 nm corresponding to a retardance of about 40 nm. Here, $n_{\parallel}$ and $n_{\perp}$ are refractive indices parallel and perpendicular, respectively, to the orientation induced by shearing and surface treatment. To enable device design for a targeted application, the retardance value can be optimized by adjusting film thickness and optical birefringence. The sharp change in birefringence at $\lambda \leq 600$ nm is caused by anisotropic light absorption prescribed by the Kramers−Kronig relation, namely, the refractive index along the absorption direction increasing faster toward a shorter wavelength than the orthogonal. The full MMt data and the model are provided in Figure S10. The obtained optical birefringence is less than that of crystalline anatase due in part to imperfect alignment and in part to the inferior form birefringence caused by sintering.

The preferred crystallographic orientation evidenced by Figure 3 can be combined with morphological and optical characterization data to offer a physical picture of the sintered product, as depicted in Figure 1g. Nanorod precursors sinter into distinguishable, low-aspect-ratio crystalline grains, identifiable from SEM in Figure 1d. Sintering results in preferred lateral growth of crystalline grains is shown by the X-ray diffraction data in Figure 2. Together, the X-ray diffraction data revealing the observed shear-induced orientation combined with the measured optical birefringence, shown in Figure 4d, confirm that the domains exhibit preferred uniaxial order of their crystallographic *c*-axes or equivalently their nematic directors. In a nutshell, the collection of grains shown in Figure 1g can be interpreted as a nematic superstructure, culminating in one of the targeted mesomorphic ceramics.

Prior to the presently reported methodology based on lyotropic liquid crystals, LLC, physical vapor deposition has been widely practiced particularly for sculptured TiO_2 films by GLAD[10] and serial bideposition, SBD,[37] with varying degrees of sophistication. Compared with GLAD and the refinement hereof, the LLC approach demonstrated here is cost-effective, while enjoying process scalability and superior optical transparency from 500 to 2500 nm through micron-thick films. The transparency shown in Figure 4d is in contrast with that in Figure 8 of ref 37, presumably because of the smaller pores through the LLC film compared with the SBD film. In the realm of GLAD, it is widely accepted that form birefringence has been exploited to achieve the maximum Δn value up to 0.22 at 550 nm[10,37] with XRD analysis in support of sintering, albeit not explicitly identified as such, at a processing temperature of up to 1000 °C. In addition, blade coating of the stable colloidal suspension of $LaPO_4$ nanorods followed by evaporating off ethylene glycol at 140 °C with subsequent thermal annealing at

https://dx.doi.org/10.1021/acsanm.0c01668
ACS Appl. Nano Mater. XXXX, XXX, XXX−XXX

500 °C for 2 h, but without referring to sintering, produced a well-oriented solid film with a film thickness of up to 1 μm.[18] The resulting Δn value at 0.13 ± 0.01 is attributed to a combination of intrinsic and form birefringence likely to be contributed by superior nanorod alignment by blade coating while bypassing sintering.[38] The modest Δn value observed herein has left much to be desired by implementing sintering process optimization as a test of the hypothesis that sintering improves the film's mechanical strength at the expense of optical birefringence at elevated temperatures where the orientational order is depressed. The overall optical birefringence could also be enhanced by mechanical and thermal processing to exploit both the intrinsic birefringence of the crystalline grains and the form birefringence from the sintered structure.[37,38]

CONCLUSIONS

In summary, uniaxially oriented mesomorphic ceramics are synthesized by spontaneous assembly of nanorods forming lyotropic liquid crystals in an isotropic and volatile solvent. This is a new class of advanced materials characterized by a facile, low-cost synthesis by way of lyotropic liquid crystals in contrast to liquid-crystal-templated synthesis of nanomaterials. Manual shear of the lyotropic film prior to thermal treatments can preserve the uniaxial orientation in the sintered film over millimeter dimensions. The mesomorphic ceramics, as reported herein, exhibit a preferred orientational order of the nanoscale grains' crystallographic *c*-axes within a nematic-like superstructure, thereby resulting in optical birefringence and transparency underlying robust waveplates for polarization control of propagating light. The inorganic particle shape, surface functionality, and choice of the suspending solvent all provide access to lyotropic phase stability, mesoscopic organization, and particle mobility, facilitating orientation *via* external fields such as shear. Furthermore, avoiding a liquid crystal template offers a path forward toward dense and mechanically robust mesomorphic films. Above all, the bottom-up spontaneous assembly of nanoparticle precursors followed by sintering provides a scalable approach to control both morphology and anisotropy that is not readily implementable by the synthesis of textured ceramics. Such a control could offer significant benefits to catalysis and photocatalysis, where crystal faces and edges greatly influence catalytic activity, and on solid-state electronics, including piezoelectrics and thermoelectrics. Optimization of the sintering process is warranted by blade coating, for example, to arrive at the optical and mechanical properties, film thickness, and aperture desired for an intended application. The more sophisticated helical stacking of nanorods will also be attempted to create chiral superstructures for circular polarization and optical isolation.

ASSOCIATED CONTENT

Supporting Information

The Supporting Information is available free of charge at https://pubs.acs.org/doi/10.1021/acsanm.0c01668.

X-ray diffraction pattern, TEM images, and TGA curves of the as-synthesized nanorods; POM images of 60 wt % oleic acid-capped TiO_2 in chlorobenzene sandwiched between two glass substrates without surface treatment upon stage rotation; grain size distribution of the sample sintered at 800 °C; SEM image of TiO_2 sintered at 800 °C with the presence of angular facets and cross section with a similar morphology; X-ray diffraction pattern of TiO_2 nanorods treated at 400, 600, and 800 °C; POM image of uniaxially aligned oleic acid-capped TiO_2 nanorods at 60 wt % in chlorobenzene sandwiched between one quartz substrate with surface treatment and the other without; SEM image of the surface of microscopically shear-aligned TiO_2 nanorods sintered at 800 °C; and plots of Mueller matrix elements (with an enlarged M12 element for the sample region and air-gap region) and refractive indices of samples sintered at 800 °C *vs* wavelength acquired from ellipsometry (PDF)

AUTHOR INFORMATION

Corresponding Author

Mitchell Anthamatten − *Chemical Engineering Department, Advanced Materials for Photonics and Lasers, University of Rochester, Rochester, New York 14627-0166, United States;* orcid.org/0000-0002-7763-9465; Email: mitchell.anthamatten@rochester.edu

Authors

Wenshi Zhang − *Chemical Engineering Department, Advanced Materials for Photonics and Lasers, University of Rochester, Rochester, New York 14627-0166, United States;* orcid.org/0000-0002-0301-2256

Shaw H. Chen − *Chemical Engineering Department, Advanced Materials for Photonics and Lasers, University of Rochester, Rochester, New York 14627-0166, United States;* orcid.org/0000-0003-4191-9817

James N. Hilfiker − *J. A. Woollam Co., Inc., Lincoln, Nebraska 68508, United States*

Complete contact information is available at: https://pubs.acs.org/10.1021/acsanm.0c01668

Author Contributions

S.H.C. and M.A. initiated the idea and process design for synthesizing mesomorphic ceramics based on spontaneous lyotropic liquid crystal formation of nanorods in isotropic solvents; they also supervised experimental implementation and material characterization by W.Z. J.N.H. did the ellipsometry measurement and modeling. The manuscript was written primarily by M.A. and S.H.C. with W.Z.'s and J.N.H.'s contributions. All authors have approved the final version of the manuscript as submitted.

Funding

The financial support of this research by the Center on Advanced Materials for Photonics and Lasers by a University of Rochester Research Award and the Technology Development Fund is gratefully acknowledged. The National Science Foundation is gratefully acknowledged for support for the acquisition of an X-ray diffractometer (CHE-1725028) and for a variable angle spectroscopic ellipsometer (CBET-1827904).

Notes

The authors declare no competing financial interest.

ACKNOWLEDGMENTS

The authors appreciate the advice and technical discussion with Tom Baur of Meadowlark Optics, Inc. in Frederick, Colorado, Professor Stephen Kelly at the University of Hull, UK, Professor Gary Messing at Pennsylvania State University, and Dr. Michael Pierce at Rochester Institute of Technology, as well as Xinquan Cheng's assistance in the synthesis of oleic acid-capped nanorods following literature procedures. The financial support

of this research by the Center on Advanced Materials for Photonics and Lasers by a University of Rochester Research Award and the Technology Development Fund is gratefully acknowledged. Wenshi Zhang appreciates a Kwang-Yu and Lee-Chien Wang Fellowship for her Ph.D. education at the University of Rochester.

REFERENCES

(1) Mitchell, K. J.; Radwell, N.; Franke-Arnold, S.; Padgett, M. J.; Phillips, D. B. Polarisation structuring of broadband light. *Optic Express* **2017**, *25*, 25079−25089.
(2) Zhao, X.; Yao, Y.; Sun, Y.; Liu, C. Circle Polarization Shift Keying With Direct Detection for Free-Space Optical Communication. *J. Opt. Commun. Netw.* **2009**, *1*, 307−312.
(3) Xu, P.; Zhang, H.; Qian, H.; Chen, B.; Jiang, X.; Wu, Y.; Liu, X.; Liu, X.; Yang, Q. Polarized light source based on graphene-nanoribbon hybrid structure. *Opt. Commun.* **2017**, *395*, 76−81.
(4) Huang, L.; Xu, J.; Ye, J.; Liu, X.; Zhang, H.; Wang, X.; Zhou, P. Power Scaling of Linearly Polarized Random Fiber Laser. *IEEE J. Sel. Top. Quant. Electron.* **2018**, *24*, 1−8.
(5) Koike-Tani, M.; Tani, T.; Mehta, S. B.; Verma, A.; Oldenbourg, R. Polarized Light Microscopy in Reproductive and Developmental Biology. *Mol. Reprod. Dev.* **2015**, *82*, 548−562.
(6) Walther, J.; Golde, J.; Kirsten, L.; Tetschke, F.; Hempel, F.; Rosenauer, T.; Hannig, C.; Koch, E. In vivo imaging of human oral hard and soft tissues by polarization-sensitive optical coherence tomography. *J. Biomed. Optic.* **2017**, *22*, 121717.
(7) Chen, H. M. P.; Ou, J. J.; Chen, S. H. Glassy Liquid Crystals as Self-Organized Films for Robust Optoelectronic Devices. *Nanoscience with Liquid Crystals,NanoScience and Technology*; Springer, 2014; pp 179−208.
(8) Chen, S. H.; Katsis, D.; Schmid, A. W.; Mastrangelo, J. C.; Tsutsui, T.; Blanton, T. N. Circularly polarized light generated by photoexcitation of luminophores in glassy liquid-crystal films. *Nature* **1999**, *397*, 506−508.
(9) Hawkeye, M. M.; Brett, M. J. Glancing angle deposition: Fabrication, properties, and applications of micro- and nanostructured thin films. *J. Vac. Sci. Technol., A* **2007**, *25*, 1317−1335.
(10) Barranco, A.; Borras, A.; Gonzalez-Elipe, A. R.; Palmero, A. Perspectives on oblique angle deposition of thin films: From fundamentals to devices. *Prog. Mater. Sci.* **2016**, *76*, 59−153.
(11) Ikesue, A.; Aung, Y. L. Origin and Future of Polycrystalline Ceramic Lasers. *IEEE J. Sel. Top. Quant. Electron.* **2018**, *24*, 1−7.
(12) Kitajima, S.; Yamakado, K.; Shirakawa, A.; Ueda, K.-i.; Ezura, Y.; Ishizawa, H. Yb^{3+}-doped CaF_2-LaF_3 ceramics laser. *Opt. Lett.* **2017**, *42*, 1724−1727.
(13) Messing, G. L.; Poterala, S.; Chang, Y.; Frueh, T.; Kupp, E. R.; Watson, B. H.; Walton, R. L.; Brova, M. J.; Hofer, A.-K.; Bermejo, R.; Meyer, R. J. Texture-engineered ceramics-Property enhancements through crystallographic tailoring. *J. Mater. Res.* **2017**, *32*, 3219−3241.
(14) Zhang, Z.; Duan, X.; Qiu, B.; Yang, Z.; Cai, D.; He, P.; Jia, D.; Zhou, Y. Preparation and anisotropic properties of textured structural ceramics: A review. *J. Adv. Ceram.* **2019**, *8*, 289−332.
(15) Geng, Y.; Trajkovska, A.; Culligan, S. W.; Ou, J. J.; Chen, H. M. P.; Katsis, D.; Chen, S. H. Origin of strong chiroptical activities in films of nonafluorenes with a varying extent of pendant chirality. *J. Am. Chem. Soc.* **2003**, *125*, 14032−14038.
(16) Kato, T.; Mizoshita, N.; Kishimoto, K. Functional liquid-crystalline assemblies: Self-organized soft materials. *Angew. Chem., Int. Ed.* **2006**, *45*, 38−68.
(17) Cozzoli, P. D.; Kornowski, A.; Weller, H. Low-temperature synthesis of soluble and processable organic-capped anatase TiO_2 nanorods. *J. Am. Chem. Soc.* **2003**, *125*, 14539−14548.
(18) Kim, J.; Peretti, J.; Lahlil, K.; Boilot, J.-P.; Gacoin, T. Optically Anisotropic Thin Films by Shear-Oriented Assembly of Colloidal Nanorods. *Adv. Mater.* **2013**, *25*, 3295−3300.
(19) Cheng, F.; Verrelli, E.; Alharthi, F. A.; Kelly, S. M.; O'Neill, M.; Kemp, N. T.; Kitney, S. P.; Lai, K. T.; Mehl, G. H.; Anthopoulos, T. Lyotropic "hairy" TiO_2 nanorods. *Nanoscale Adv.* **2019**, *1*, 254−264.
(20) Hu, H.; Wang, S.; Feng, X.; Pauly, M.; Decher, G.; Long, Y. In-plane aligned assemblies of 1D-nanoobjects: recent approaches and applications. *Chem. Soc. Rev.* **2020**, *49*, 509−553.
(21) Meseck, G. R.; Terpstra, A. S.; MacLachlan, M. J. Liquid crystal templating of nanomaterials with nature's toolbox. *Curr. Opin. Colloid Interface Sci.* **2017**, *29*, 9−20.
(22) Dessombz, A.; Chiche, D.; Davidson, P.; Panine, P.; Chanéac, C.; Jolivet, J.-P. Design of liquid-crystalline aqueous suspensions of rutile nanorods: Evidence of anisotropic photocatalytic properties. *J. Am. Chem. Soc.* **2007**, *129*, 5904−5909.
(23) Zhang, Q.; Joo, J.-B.; Lu, Z.; Dahl, M.; Oliveira, D. Q. L.; Ye, M.; Yin, Y. Self-Assembly and Photocatalysis of Mesoporous TiO_2 Nanocrystal Clusters. *Nano Res.* **2011**, *4*, 103−114.
(24) Deng, H.; Zhang, H.; Lu, Z. Dye-sensitized anatase titanium dioxide nanocrystalline with (001) preferred orientation induced by Langmuir-Blodgett monolayer. *Chem. Phys. Lett.* **2002**, *363*, 509−514.
(25) Kawakita, M.; Kawakita, J.; Uchikoshi, T.; Sakka, Y. Photoanode characteristics of dye-sensitized solar cell containing TiO_2 layers with different crystalline orientations. *J. Mater. Res.* **2009**, *24*, 1417−1421.
(26) Sun, B.; Sirringhaus, H. Surface tension and fluid flow driven self-assembly of ordered ZnO nanorod films for high-performance field effect transistors. *J. Am. Chem. Soc.* **2006**, *128*, 16231−16237.
(27) Chang, Y.; Watson, B.; Fanton, M.; Meyer, R. J.; Messing, G. L. Enhanced texture evolution and piezoelectric properties in CuO-doped $Pb(In_{1/2}Nb_{1/2})O$-3-$Pb(Mg_{1/3}Nb_{2/3})O_3$-$PbTiO_3$ grain-oriented ceramics. *Appl. Phys. Lett.* **2017**, *111*, 232901.
(28) Kimura, T. Application of texture engineering to piezoelectric ceramics—A review. *J. Ceram. Soc. Jpn.* **2006**, *114*, 15−25.
(29) Guang, M.; Xia, Y.; Wang, D.; Zeng, X.-F.; Wang, J.-X.; Chen, J.-F. Controllable synthesis of transparent dispersions of monodisperse anatase-TiO_2 nanoparticles and nanorods. *Mater. Chem. Phys.* **2019**, *224*, 100−106.
(30) Dierking, I. *Textures of Liquid Crystals*; Wiley-VCH Verlag, 2003; pp 51−54.
(31) Hong, R. Y.; Feng, B.; Cai, X.; Liu, G.; Li, H. Z.; Ding, J.; Zheng, Y.; Wei, D. G. Double-miniemulsion preparation of Fe_3O_4/poly (methyl methacrylate) magnetic latex. *J. Appl. Polym. Sci.* **2009**, *112*, 89−98.
(32) Munier, P.; Gordeyeva, K.; Bergström, L.; Fall, A. B. Directional Freezing of Nanocellulose Dispersions Aligns the Rod-Like Particles and Produces Low-Density and Robust Particle Networks. *Biomacromolecules* **2016**, *17*, 1875−1881.
(33) Apetz, R.; Bruggen, M. P. B. Transparent alumina: A light-scattering model. *J. Am. Ceram. Soc.* **2003**, *86*, 480−486.
(34) Fujiwara, H. *Spectroscopic Ellipsometry: Principles and Applications*; John Wiley & Sons, 2007.
(35) Hilfiker, J. N.; Tiwald, T. Dielectric Function Modeling. *Spectroscopic Ellipsometry for Photovoltaics*; Springer, 2018; pp 115−153.
(36) Hilfiker, J. N.; Johs, B.; Herzinger, C. M.; Elman, J. F.; Montbach, E.; Bryant, D.; Bos, P. J. Generalized spectroscopic ellipsometry and Mueller-matrix study of twisted nematic and super twisted nematic liquid crystals. *Thin Solid Films* **2004**, *455−456*, 596−600.
(37) van Popta, A. C.; Cheng, J.; Sit, J. C.; Brett, M. J. Birefringence enhancement in annealed TiO_2 thin films. *J. Appl. Phys.* **2007**, *102*, 013517.
(38) Kim, J.; Martinelli, L.; Lahlil, K.; Boilot, J.-P.; Gacoin, T.; Peretti, J. Optimized combination of intrinsic and form birefringence in oriented $LaPO_4$ nanorod assemblies. *Appl. Phys. Lett.* **2014**, *105*, 061102.

https://dx.doi.org/10.1021/acsanm.0c01668
ACS Appl. Nano Mater. XXXX, XXX, XXX−XXX